Climatology of Tropical Cyclogenesis in the North Atlantic (1948–2004)

RON MCTAGGART-COWAN

Numerical Weather Prediction Research Section, Meteorological Service of Canada, Dorval, Quebec, Canada

GLENN D. DEANE

Department of Sociology, University at Albany, State University of New York, Albany, New York

LANCE F. BOSART

Department of Earth and Atmospheric Sciences, University at Albany, State University of New York, Albany, New York

CHRISTOPHER A. DAVIS

Mesoscale and Microscale Meteorology, National Center for Atmospheric Research, Boulder, Colorado*

THOMAS J. GALARNEAU JR.

Department of Earth and Atmospheric Sciences, University at Albany, State University of New York, Albany, New York

(Manuscript received 26 April 2007, in final form 27 July 2007)

ABSTRACT

The threat posed to North America by Atlantic Ocean tropical cyclones (TCs) was highlighted by a series of intense landfalling storms that occurred during the record-setting 2005 hurricane season. However, the ability to understand—and therefore the ability to predict—tropical cyclogenesis remains limited, despite recent field studies and numerical experiments that have led to the development of conceptual models describing pathways for tropical vortex initiation. This study addresses the issue of TC spinup by developing a dynamically based classification scheme built on a diagnosis of North Atlantic hurricanes between 1948 and 2004. A pair of metrics is presented that describes TC development from the perspective of external forcings in the local environment. These discriminants are indicative of quasigeostrophic forcing for ascent and lower-level baroclinicity and are computed for the 36 h leading up to TC initiation. A latent trajectory model is used to classify the evolution of the metrics for 496 storms, and a physical synthesis of the results yields six identifiable categories of tropical cyclogenesis events. The nonbaroclinic category accounts for 40% of Atlantic TCs, while events displaying perturbations from this archetype make up the remaining 60% of storms. A geographical clustering of the groups suggests that the classification scheme is identifying fundamentally different categories of tropical cyclogenesis. Moreover, significant differences between the postinitiation attributes of the classes indicate that the evolution of TCs may be sensitive to the pathway taken during development.

1. Introduction

The power of tropical cyclones (TCs) and the threat that they pose to populations and infrastructures in coastal areas was devastatingly illustrated by the record-setting 2005 Atlantic Ocean hurricane season. That season produced not only the most named TCs in history (27) but also the costliest [e.g., Hurricane Katrina cost an estimated $81 billion (U.S. dollars; Knabb et al. 2005)], the third-deadliest since the turn of the twentieth century [e.g., Hurricane Katrina, with an estimated 1833 fatalities (Knabb et al. 2005)], and the deepest [e.g., Hurricane Wilma, with a minimum mean sea level pressure estimated at 882 hPa (Pasch et al. 2005)] hurricanes recorded by the U.S. National Hurricane Center (NHC).

* The National Center for Atmospheric Research is sponsored by the National Science Foundation.

Corresponding author address: Ron McTaggart-Cowan, 2121 Trans-Canada Highway, Floor 5, Dorval, Québec H9P 1J3, Canada.
E-mail: ron.mctaggart-cowan@ec.gc.ca

DOI: 10.1175/2007MWR2245.1

Despite seasonal predictions of above-average hurricane activity for the subsequent season, based both on model diagnostics and on climate statistics (NOAA 2006), 2006 resulted in only 10 named TCs in the North Atlantic basin. This dramatic interseasonal variability is noteworthy but not unique in the record, and it serves to highlight the fact that despite the significant improvements that have been made in hurricane track forecasting (Burpee et al. 1996; Goerss 2007)—and much more modest improvements that have been achieved in intensity prediction (DeMaria et al. 2005, 2007)—many questions still surround the development of TCs (e.g., Elsberry et al. 1992; Marks et al. 1998). This issue was highlighted by the recommendation of those attending the Sixth International Workshop on Tropical Cyclones that research be focused on TC structural changes during genesis and on finding objective ways to quantify the influence of trough forcing on TC outflow (IWTC-VI 2006). This investigation develops a dynamically based categorization scheme for tropical cyclogenesis in the North Atlantic basin. The result provides an objective method for framing studies and discussions of tropical cyclogenesis in analyses, forecast models, and climate prediction systems.

Many advanced theories describing the physical and dynamical processes responsible for the development of TCs have been proposed in recent literature. These can be broadly categorized as those that emphasize "pure" tropical (nonbaroclinic) features and forcings and those that implicate external influences, typically of midlatitude origin, in tropical cyclogenesis.

The former group of development models favors convectively driven development pathways and includes the thermodynamically focused studies of Rotunno and Emanuel (1987) and Emanuel and Rotunno (1989), wherein the wind-induced surface heat exchange (WISHE) model is developed to demonstrate the effectiveness of surface fluxes in raising the lower-level equivalent potential temperature (θ_e) to a value capable of sustaining a mesoscale convective vortex (MCV). Recent studies by Hendricks et al. (2004), Montgomery et al. (2006), and Sippel et al. (2006) build on the work of Chen and Frank (1993) to show how these MCVs can be created and sustained by individual convective elements called "vortical hot towers" (Simpson et al. 1998). High-resolution modeling work by Davis and Bosart (2001), Hendricks et al. (2004), and Montgomery et al. (2006) shows how numerous convective cells with lifetimes on the order of 1 h can combine to create a quasi-steady heating rate on the primary MCV scale. Field observations are used by Ritchie and Holland (1993, 1997) and Simpson et al. (1997) to develop models of tropical cyclogenesis that focus on the stochastic coalescence of convectively generated vortex features in a favorable synoptic environment created by the monsoon trough. This combination of scales—from convective to synoptic—is a key element of conceptual models that describe the TC development pathways that depart from the pure tropical form.

The importance of these scale interactions has received attention recently in the form of the tropical transition (TT) development model defined by Davis and Bosart (2004). Building on studies of a 1975–93 composite of TC developments (Bracken and Bosart 2000) and the initiation of Hurricane Diana (1984) (Bosart and Bartlo 1991; Davis and Bosart 2001, 2002), Davis and Bosart (2004, 2006) describe the importance of upper-level trough forcing and convectively driven diabatic potential vorticity (PV) and momentum redistribution in enhancing MCV strength and in the reduction of the near-storm vertical wind shear implied by the presence of the midlatitude trough, or "PV tail." Two categories of TT are described by Davis and Bosart (2004): weak extratropical cyclone (WEC) and strong extratropical cyclone (SEC). Storms classified as SEC cases involve extratropical baroclinic precursors of sufficient strength (surface winds near 10 m s^{-1}) to trigger the WISHE process. Weak extratropical cyclone developments form from weaker initial baroclinic vortices and require a sustained convective outbreak—generally induced by the quasigeostrophic forcing for ascent downshear of the trough—to generate near-surface winds strong enough to raise θ_e values through surface fluxes.

Another model of tropical cyclogenesis that involves lower-level baroclinicity has been developed to describe Cape Verde hurricane initiation (Simpson and Riehl 1981) west of the African coast. One of the key ingredients for this development pathway is the presence of a midlevel easterly jet (MLEJ) that satisfies the Charney and Stern (1962) condition for combined barotropic–baroclinic instability (a vanishing-time mean north–south PV gradient). This strong MLEJ is sustained by episodic injections of warm, well-mixed, dust-laden boundary layer air into the Saharan air layer (SAL; Carlson and Prospero 1972) over the eastern equatorial Atlantic. A strong meridional temperature gradient is established between the SAL and cooler midlevel air of oceanic origins to the south, giving rise to an MLEJ in which wind speeds exceed 10 m s^{-1} at 700 hPa. Karyampudi and Pierce (2002) use a vorticity budget analysis of recent Cape Verde developments to show that the combined effects of convection-induced

vortex stretching and cyclonic vorticity advection on the equatorward side of the MLEJ are sufficient to promote cyclogenesis in two of the three cases studied. Using a compositing approach, Bracken and Bosart (2000) show that vorticity advection on the southern flank of the Atlantic subtropical anticyclone can promote TC development in the MLEJ entrance. A three-stage life cycle of easterly waves on the cyclonic shear side of the MLEJ is proposed by Berry and Thorncroft (2005), following their study of the strong wave that led to the development of Hurricane Alberto (2000). Because of the requirement for a strong lower-level temperature gradient in this model, its applicability is generally confined to the eastern Atlantic basin.

Geographical constraints on tropical cyclogenesis are employed by Elsner et al. (1996) to develop a climatology of tropical cyclogenesis for the Atlantic. Using an advanced statistical algorithm known as partially adaptive classification trees (Shih 1993) and NHC best-track positional information, Elsner et al. (1996) split 1950–93 hurricane developments into "tropical only" and "baroclinically influenced" categories based on the geographical locations of the first reports of tropical depression and hurricane strengths in the best track. The Elsner et al. (1996) study is founded on a subjective classification involving the same two categories over a similar period performed by Hess et al. (1995). The latter study focuses on an application of the categorized dataset to the extended range prediction of tropical cyclogenesis from synoptic-scale indicators in seasonal forecast models.

The current study is similar to that of Elsner et al. (1996) in objective but differs significantly in method. Our goal is to design a classification scheme for tropical cyclogenesis events based on physically meaningful discriminants that represent important underlying processes and mechanisms, thereby freeing the analysis of imposed geographical constraints. We define no limit on the number of unique tropical cyclogenesis categories a priori, but like Elsner et al. (1996), we strive to replicate the classifications that would be identified by an experienced atmospheric scientist well versed in the tropical development theories described in this section. An objective dynamically based climatology of tropical cyclogenesis will have the potential for a broad range of applications including investigations of seasonal predictions (as performed by Hess et al. 1995) and climate simulations. In real time, hurricane genesis classification could be applied as a forecasting tool given the ever-increasing quality of high-resolution gridded analyses.

This study begins with a description in section 2 of the datasets and the diagnostic methodology. Section 3 describes the latent trajectory modeling technique employed to develop the objective categorization scheme. Selected results from the climatological classification are presented in section 4. The study concludes in section 5 with a summary and discussion of the findings.

2. Data and diagnostics methodology

a. Datasets

All of the diagnostics presented in this study are computed from the National Centers for Environmental Prediction–National Center for Atmospheric Research reanalysis dataset (NCEP–NCAR reanalysis) with a 2.5°-latitude–longitude grid spacing (Kalnay et al. 1996; Kistler et al. 2001). Data from 1948–2004 are used, with the 2005 season intentionally excluded to allow for the planned development of a diagnostic categorization strategy and its independent verification against new high-resolution analysis data from the NCEP Global Forecast System. One of the primary benefits of using a gridded reanalysis dataset for the development of a classification scheme is that it allows for the definition of a set of dynamically based categories. However, the 2.5° grid spacing of the NCEP–NCAR reanalysis is clearly insufficient to resolve the nature of individual tropical vortices themselves, especially during the early stages of development. Throughout this study, we therefore focus on the near-storm synoptic environment and its influence on the nascent TC. Given the resolvable scale of these features in the NCEP–NCAR reanalysis dataset, we have included data collected before the International Geophysical Year of 1957 (IGY-1957) and the advent of the satellite era (approximately 1979) in order to allow the statistical analysis (section 3) to operate on the largest number and broadest range of cases possible.

In this study, the diagnostics considered as "metrics" representative of the tropical cyclogenesis pathway followed during development are computed using only high-confidence type-A variables with the exception of the irrotational component of the full wind field, a lower-quality type-B variable. Type-A variables are strongly influenced by observations in NCEP–NCAR reanalysis data, while type-B variables are more closely related to the model fields used as the background state during NCEP–NCAR reanalysis data assimilation (Kalnay et al. 1996). Kistler et al. (2001) show that much of the analysis error—defined by forecast increments and anomaly correlations of the 500-hPa height field—in both early (before 1958) and presatellite (before 1979) grids is concentrated over the Southern Hemisphere

oceans. The Northern Hemisphere, and particularly the North Atlantic basin, are relatively well handled throughout the NCEP–NCAR reanalysis dataset. The authors use a pair of case studies [the Thanksgiving storm of 1950 (Smith 1950; Phillips 1958) and the North Sea Gale of 1953] to show that even pre-IGY-1957 analyses are well represented by the data assimilation scheme used in the reanalysis system. These findings increase confidence in diagnostics computed from NCEP–NCAR reanalysis data, at least over the region of interest for this study.

The quality of the other primary dataset used here, the NHC best-track archive, is also variable over the period of 1948–2004. While the introduction of regular reconnaissance missions in 1944 greatly enhanced the accuracy of the best-track record after that time, other technological advances including satellite track and intensity estimate tools (Dvorak 1975) and dropsondes [implemented in 1982; impacts evaluated by Burpee et al. (1996)] have also improved the quality of the archive. Since the best-track data are used in this study only to locate the center of the storm, TCs close enough to the North American continent for aircraft sampling will be well represented. The positions of those located farther eastward will contain more uncertainty, especially in the presatellite era when ship observations comprose the majority of the tracking input data (Landsea 2007). Given the low resolution of the NCEP–NCAR reanalysis dataset, however, small errors in the locations of the TC centers are unlikely to have a dramatic impact on the results of the diagnostics computed in this study. To capture the full spectrum of tropical development events, and consistent with a designed lack of a priori assumptions regarding the number or nature of tropical cyclogenesis categories, cyclones that remain unnamed and those designated subtropical are considered in this study. However, to eliminate cases in which the cyclogenesis stage of the TC life cycle is missing from the archive—and in keeping with Elsner et al. (1996)—only storms with estimated winds in the first best-track report less than tropical storm strength (17 m s^{-1}) are retained (95 of the 591 storms in the 1948–2004 best-track record are rejected by this condition, leaving 496 TCs in this study).

b. Diagnostic analysis

To develop a dynamically based categorization scheme for tropical cyclogenesis, a set of representative diagnostic fields must be computed for each TC. Because the genesis process occurs on a time scale of days, an instantaneous snapshot of the near-storm environment is insufficient to capture the full range of cyclogenesis events. The limitations of a single time analysis are addressed by Elsner et al. (1996) through the use of the central location of the TC at the onset of both the tropical storm and the hurricane (33 m s^{-1}) phases of the storm's life cycle. In this study, we consider the evolution of the near-vortex environment over the 36-h period leading up to the time of the initial storm report in the best-track record (hereinafter referred to as T_o).

To obtain a set of storm-following diagnostics, a series of vortex-center coordinates is required over the period $T_o - 36$ h to T_o. (Here $T_o - 36$ h represents the analysis time 36 h before T_o; other pre- and post-T_o times are indicated similarly.) These are obtained using the geostrophic steering flow between 1000 and 400 hPa [found by Dong and Neumann (1986) to be the optimal steering layer in the North Atlantic for systems of tropical storm strength] computed at 6-hourly intervals from the NCEP–NCAR reanalysis for a torroidal region with an inner radius of 2° and an outer radius of 8°, centered on the storm location. Dong and Neumann (1986) show that this computation of the steering flow for a vortex of tropical storm strength yields errors of approximately 300 km—just over one grid length in the NCEP–NCAR reanalysis—in a 36-h period. This method has been chosen over a feature-tracking approach because the weak intensity and mesoscale extent of the TCs at T_o imply that they are poorly represented in the coarse-resolution NCEP–NCAR reanalysis. When higher-resolution analysis or reanalysis data capable of consistently identifying tropical vortices before T_o become available, a feature-tracking algorithm may become the method of choice for the storm back-trajectory calculation.

For each analysis time, between $T_o - 36$ h and T_o, a set of global diagnostics (Table 1) is generated using high-order accuracy spherical harmonic computations (Adams and Swarztrauber 1997). The results of these diagnostics are interpolated onto a storm-centered grid in cylindrical coordinates (north up) with azimuthal and radial grid spacings of 5° and 1°, respectively. The maximum radius of each resulting storm-centered "dial" is 10°. The dials are plotted in arbitrary groupings of "basic" and "advanced" diagnostics (Table 1, where the classifications are loosely based on the regularity with which the individually derived diagnostics appear in the recent literature and synoptic discussions) and are stored in a database that contains almost 20 000 images for the 1948–2004 period. Figures 1 and 2 show examples of the dial plots for Hurricane Michael at $T_o -$ 24 h, valid at 1200 UTC 14 October 2000. A Web interface has been developed for investigators and the general audience (accessible online at http://www.

TABLE 1. Diagnostic fields computed from the NCEP–NCAR reanalysis for all 496 storms in this study. Plots of these quantities are available via the Web interface (http://www.atmos.albany.edu/facstaff/rmctc/ttclim/indexd.php).

Diagnostic	Chart type	Figures	Text symbol
DT[a] potential temperature	Basic	1a	
DT pressure	Advanced	2a	
DT winds	Basic	1a, 2a	
Eady model DT potential temperature anomaly[b]	Advanced	2d	
Lower-level nondivergent wind (850–700 hPa)	Basic	1c	
Lower-level relative vorticity (850–700 hPa)	Basic	1c	
Lower-level thickness (1000–700 hPa)	Basic	1b	Th
Lower-level winds (1000–700 hPa)	Basic	1b	
Midlevel relative humidity (850–400 hPa)	Basic	1d	
Potential intensity (Bister and Emanuel 2002)	Advanced	2b	
Upper-level irrotational winds (400–200 hPa)	Advanced	2c	
Upper-level Q vector convergence (400–200 hPa)	Basic	1d	Q
Upper-level Q vectors (400–200 hPa)	Basic	1d	
Upper-level R_d[c] (400–200 hPa)	Advanced	2c	
Wind shear (DT-850 hPa)	Advanced	2b	

[a] DT is defined as the 1.5-PVU surface, where 1 PVU = 10^{-6} m^2 kg^{-1} s^{-1}.

[b] The Eady-model anomaly is defined as DT potential temperature departure from an atmosphere that conforms to the Eady (1949) basic state. A detailed description of this diagnostic is contained in McTaggart-Cowan et al. (2006).

[c] The Rossby penetration depth R_d is defined as $R_d = L(f_o^2/N^2)^{1/2}$, where f_o is a reference Coriolis parameter (20°N), L is a horizontal length scale (1000 km), and N^2 is the square of the Brunt–Väisälä frequency.

atmos.albany.edu/facstaff/rmctc/ttclim/indexd.php). Each TC can be selected based on year and name (or storm number if the TC is not named or classified as subtropical by the NHC), and the diagnostic fields are used to create an animation sequence.

Extensive review of the plots in the database is required to select the most appropriate metrics (discriminants) for the classification scheme. The criteria for the metrics are that they must be

- representative of the synoptic-scale near-storm environment;
- dynamically significant with respect to the theories of tropical cyclogenesis reviewed in section 1; and
- different in structure, evolution, or intensity for the different "flavors" of tropical cyclogenesis identified by theoretical models and inspection of the 1948–2004 data.

The extent to which each of the diagnostic fields described in Table 1 meets each above-listed criterion is evaluated for a broad range of TCs using extensive analysis of the dial plots for 70 storms spanning the full period of the investigation (14% of the full dataset).[1] This is the sole subjective component of this study, and it will have an impact on the final TC classifications; however, this subjectivity is consistent with the stated objective of replicating the diagnosis of an experienced analyst. Two metrics are chosen because of their clear conformity to the full set of criteria: mean upper-level quasi-nondivergent Q-vector convergence and lower-level thickness asymmetry. The choice of these metrics is not unique, nor is the selection of two diagnostic fields; however, the final interpretation of the TC classes becomes increasingly difficult for larger numbers of discriminant fields (section 3). The lower-level relative vorticity, a clear measure of the strength of the precursor MCV, was considered as a metric but rejected because of the inconsistent representation of tropical vortices in the NCEP–NCAR reanalysis and the fact that it fails to conform to the third criterion above, since the weak vortices are often too poorly resolved to contain robust information about asymmetric structures.

The mean upper-level Q-vector convergence (Q) is defined as the average convergence of the 400–200-hPa Q-vector field within a 6° radius[2] of the storm center (Fig. 1d). Unlike the standard quasigeostrophic Q vector, however, the quasi-nondivergent Q vector ($\mathbf{Q}$) is computed using the nondivergent wind field

$$\mathbf{Q} = -\frac{R}{\sigma p}\left(\begin{array}{c}\dfrac{\partial \mathbf{v}_{\mathrm{nd}}}{\partial x}\cdot\boldsymbol{\nabla}_p T \\ \\ \dfrac{\partial \mathbf{v}_{\mathrm{nd}}}{\partial y}\cdot\boldsymbol{\nabla}_p T\end{array}\right), \tag{1}$$

where $\mathbf{v}_{\mathrm{nd}}$ is the vector nondivergent wind, the $\boldsymbol{\nabla}_p$ operator computes gradients on a pressure surface, T and p are air temperature and pressure, respectively, R is the gas constant for dry air, and σ is the static stability. The complete development of this quantity is the sub-

[1] The 70-storm diagnostic set was chosen based on the authors' familiarity with selected events, augmented by random sampling from the online database.

[2] The 6° radius is chosen as a region large enough to encompass most of the vortex-steering flow (Miller 1958; Dong and Neumann 1986) while excluding forcings that occur on the extreme periphery of the developing circulation based on the diagnostic evaluation described above.

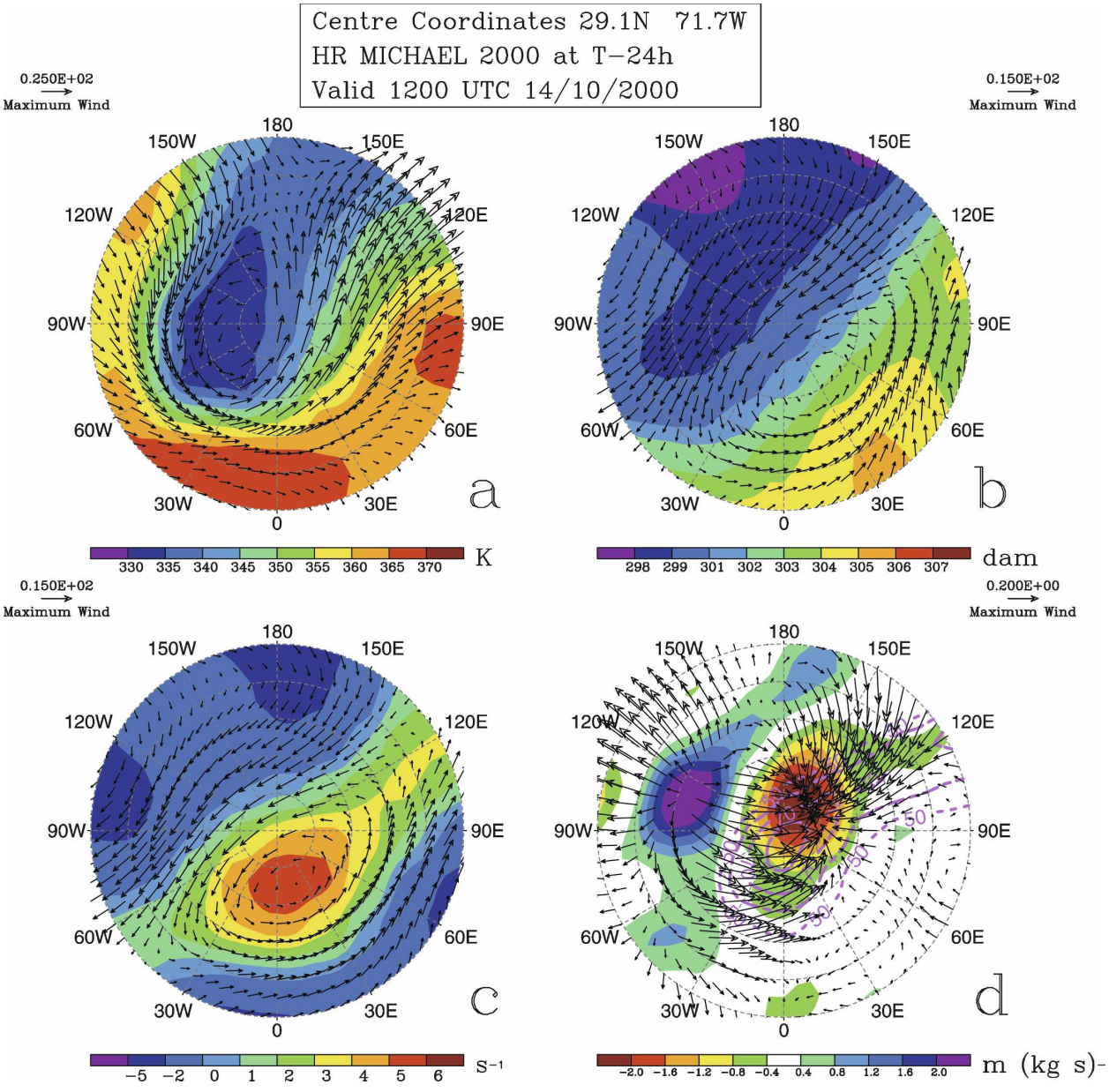

FIG. 1. Basic diagnostic dial plots for Hurricane Michael at $T_o - 24$ h, valid at 1200 UTC 15 Oct 2000. (a) Dynamic tropopause (DT; see Table 1) potential temperature (5-K contour intervals as shown on the color bar) and winds [arrows (m s^{-1}), with the reference vector at the top-left-hand corner of the panel]. (b) A 1000–700-hPa thickness (1-dam contour intervals as shown on the color bar) and mean 1000–700-hPa winds [arrows (m s^{-1}), with the reference vector at the top-right-hand corner of the panel]. (c) Mean 850–700-hPa relative vorticity ($\times 10^{-5}$ s^{-1} at intervals of 2.5×10^{-5} s^{-1} below 0 s^{-1} and 1×10^{-5} s^{-1} above, as indicated on the color bar) and mean 850–700-hPa nondivergent winds [arrows (m s^{-1}), with the reference vector at the top-left-hand corner of the plot]. (d) Mean 400–200-hPa Q-vector divergence with Q vectors computed as described by (1) ($\times 10^{-12}$ m kg^{-1} s^{-1} at 0.4×10^{-12} m kg^{-1} s^{-1} intervals as shown on the color bar), mean 840–400-hPa relative humidity (dashed magenta contours at 10% intervals at and above 50% humidity, with longer dashes for larger values), and mean 400–200-hPa nondivergent wind Q vectors [arrows (kg^{-1} s^{-1}), with the reference vectors at the top-right-hand corner of the plot].

ject of a study in preparation. Conceptually, this casting of the Q-vector equation behaves similarly to the conventional form with slaved height replaced by slaved vorticity (Warn et al. 1995; Nielsen-Gammon and Gold 2008); however, this diagnostic has distinct advantages over the former in terms of both global applicability and smoothness. The Q vector defined by (1) does not become invalid as the Rossby number (R_o) approaches

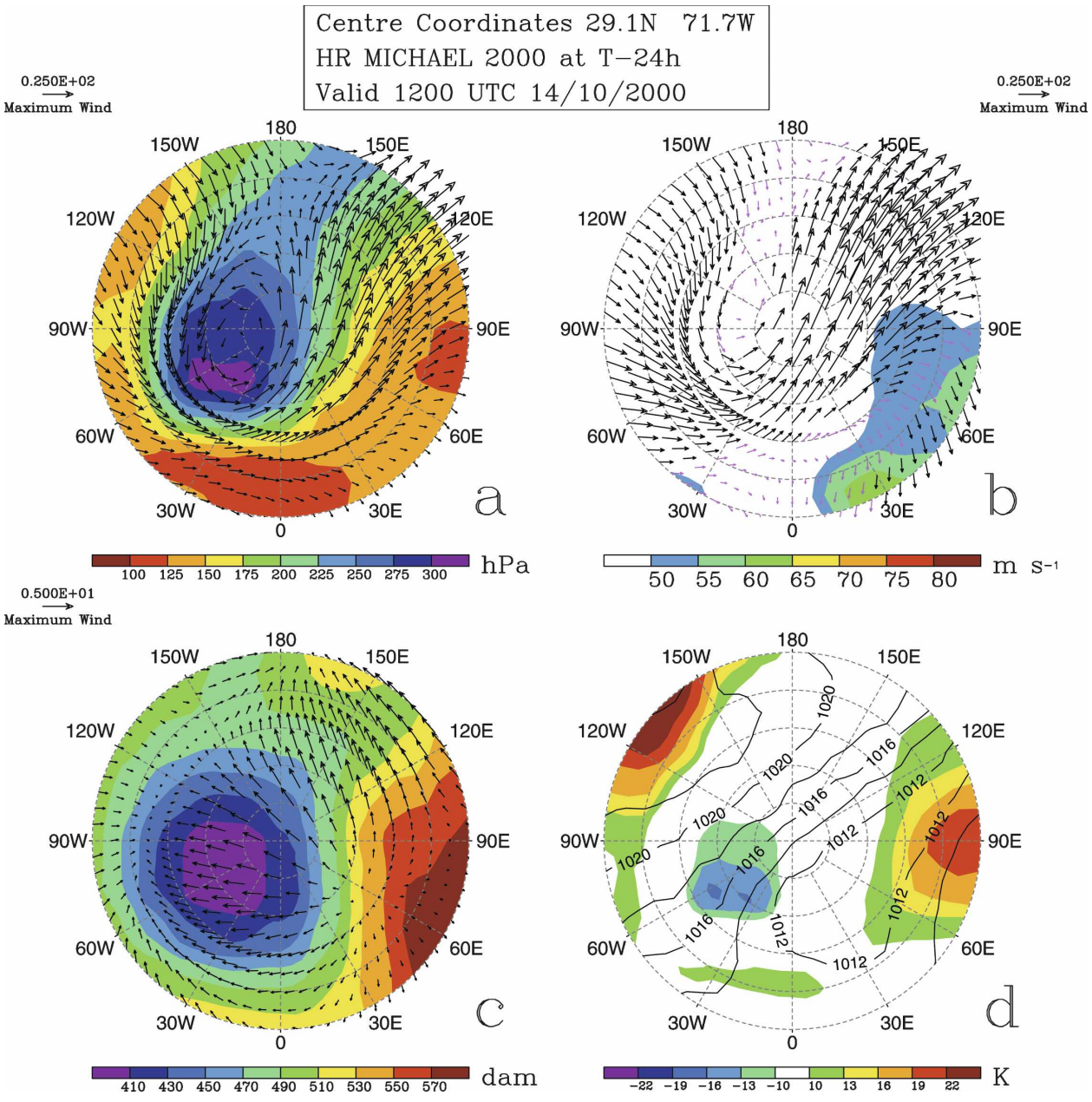

FIG. 2. Advanced diagnostic dial plots for Hurricane Michael at T_o − 24 h, valid at 1200 UTC 15 Oct 2000. (a) The DT pressure (25-hPa contour intervals as shown on the color bar) and winds [arrows (m s^{-1}), with the reference vector at the top-left-hand corner of the panel]. (b) Potential intensity computed using the method of Bister and Emanuel (2002) (5 m s^{-1} contour intervals as shown on the color bar) and vertical wind shear between the DT and 850 hPa [arrows (m s^{-1}), with the reference vector at the top-right-hand corner of the panel]. (c) Mean 400–200-hPa Rossby penetration depth (R_d) as described in Table 1 (20-dam intervals as indicated on the color bar) and 400–200-hPa irrotational winds [arrows (m s^{-1}), with the reference vector at the top-left-hand corner of the panel]. (d) The DT potential temperature anomaly as defined by the departure from an Eady (1949) basic-state atmosphere as described in Table 1 (3-K contour intervals as shown on the color bar) and mean sea level pressure (black contours at 2-hPa intervals).

unity in convective outflow and near the equator.[3] This attribute makes (1) preferable for use in studies of tropical cyclogenesis. Notwithstanding the nondivergent formulation used here, typical velocity (10 m s^{-1}) and length (1000 km) scales yield R_o values of 0.26 and 0.40 at 15° and 10°N, respectively, implying that even the standard quasigeostrophic equations are valid

[3] The $R_o = (U/fL)$, where f is the local Coriolis parameter and U and L are characteristic velocity and length scales, respectively.

throughout the main development region (MDR).[4] The use of $\mathbf{v}_{nd}$ in (1) also reduces noise in the computation of the Q vectors, since small-scale features project more heavily onto the geostrophic wind and pressure fields than they do onto the smoother nondivergent wind and vorticity fields. Given the low value of the Coriolis parameter in the tropics, any noise can create unrealistic geostrophic wind speeds even at latitudes where quasigeostrophic theory is strictly valid; this problem is overcome using the nondivergent Q-vector casting in (1).

To first order, the Q-vector metric discriminates between systems that develop in a purely tropical atmosphere (low values of Q) and those that experience upper-level forcing from a trough. Early studies on such features, then known as tropical upper-tropospheric troughs (TUTTs), were performed by Sadler (1976, 1978). More recently, tropical cyclogenesis events that rely on strong upper-level dynamic forcing fall under the TT paradigm of Davis and Bosart (2004). In addition to the cyclogenetic properties of ascent through lower-level convergence and stretching, sustained uplift increases the midlevel relative humidity by adjusting the temperature profile toward dry adiabatic. This midlevel moistening limits the effectiveness of mixing-induced downdrafts in establishing a near-surface cold pool that reduces the efficiency of the convective element (Maddox 1983). The Q metric therefore serves both to represent well-resolved dynamic processes and to act as a proxy for the poorly analyzed midlevel moisture field (a type-B variable in the NCEP–NCAR reanalysis; Kistler et al. 2001).

The lower-level thickness asymmetry (Th) is defined as the maximum difference in the mean hemispheric (semicircle) 1000–700-hPa thickness values within 10° of the storm center on the dial plots (Fig. 1b), normalized by the mean thickness in the same area.[5] Unlike the B parameter of the cyclone phase space developed by Hart (2003), the axis of division between the hemispheres is not fixed, but turns so that the axis runs perpendicular to the mean thickness gradient. Storms with moderate-to-strong lower-level baroclinicity may be undergoing development along a TT pathway (Davis and Bosart 2004) or may be associated with a MLEJ (Karyampudi and Pierce 2002). Like Q, the Th metric will not allow for a detailed evaluation of the inner-core structure of the developing TC because of the resolution limitations of the NCEP–NCAR reanalysis; however, it will identify cases in which lower-level isentropic ascent works to trigger and sustain convection (Raymond and Jiang 1990). Furthermore, the lower-level vertical wind shear implied by an elevated value of the Th metric can act to organize and ventilate the convective elements (Newton 1966; Weisman and Klemp 1982). Combined, the Q and Th metrics provide a comprehensive picture of the evolution of the near-storm environment leading up to T_o.

3. Development of the classification scheme

With a pair of metrics (Q, Th) that satisfies the three criteria outlined in section 2b now identified, values of these quantities can be computed for each time increment (from $T_o - 36$ h to T_o) for all 496 storms in the database. The time series of the metrics can then be used to develop a classification scheme that discriminates between both the magnitude and the evolution of these forcings over the development phase of the TC's life cycle.

A further complication arises for the lower-level thickness field, in which discontinuity is occasionally observed among analysis times (Fig. 3). Since temporal continuity is usually one of the advantages of using a reanalysis dataset, these jumps between analysis times are disconcerting. The explanation for these oscillations appears to be related to the magnitude of the semidiurnal tide relative to the sensitivity of the thickness dials (contour intervals are 0.5 dam in Fig. 3). The 6-hourly temporal resolution of the NCEP–NCAR reanalysis corresponds to the Nyquist frequency of the semidiurnal tide, an atmospheric tide that results from a combination of the absorption of solar radiation in the upper atmosphere and fluxes of sensible and latent heat at the surface (Dai and Wang 1999).[6] The vertical structure of the semidiurnal tide is complicated, though its magnitude generally increases with height in the troposphere (Wallace and Tadd 1974); theoretical models suggest that temporal phasing may change with altitude (Lindzen and Hong 1974). The tide's effect on a highly

[4] The MDR is the rectangular area approximately 10°–20°N and 30°–85°W, where the majority of Atlantic TCs form (Goldenberg and Shapiro 1996).

[5] The 10° radius is chosen based on the diagnostic evaluation to focus on the magnitude of the environmental baroclinicity by creating a region large enough to ensure that the background gradient overwhelms small positional errors, while remaining small enough to represent the local environment of the developing vortex.

[6] The authors also discuss a diurnal tide (Chapman and Lindzen 1970) that reaches maximum amplitude up to 6 h before local noon, the effects of which are superposed on the pressure fluctuations induced by the semidiurnal tide. However, they show that the diurnal tide has a negligible influence over the tropical oceans, and the longer tidal period suggests that aliasing is not a problem for the current study.

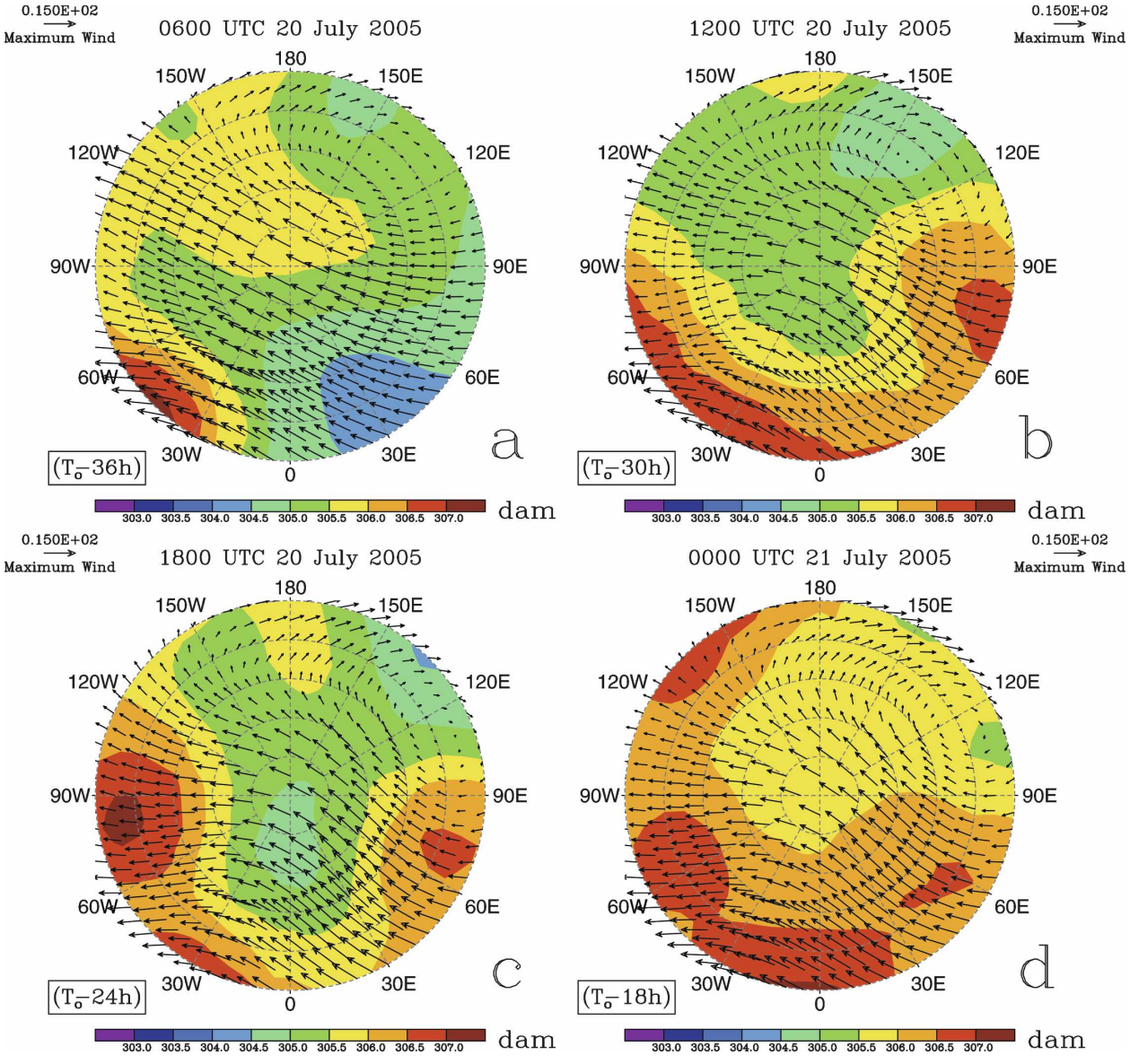

FIG. 3. Lower-level thickness (1000–700 hPa, contoured at 0.5-dam intervals as indicated on the color bar) and mean lower-level winds [1000–700 hPa; arrows (m s^{-1}), with the reference vector at the top of each panel] for Tropical Storm Franklin from T_o − 36 h to T_o − 18 h at 6-h intervals. Validity time is indicated at the top of each panel.

sensitive lower-level thickness field is therefore indeterminate but potentially large. At the surface, it manifests itself as divergence-induced 1–1.5-hPa fluctuations in the tropical mean sea level pressure field that decrease poleward and peak 2–3 h before local noon and local midnight. These times correspond to approximately 1200 and 0000 UTC in the Atlantic basin, leading to maximum amplitude in the 6-hourly jumps of the thickness analyses in this region. To avoid this aliased signal that has no theoretical correspondence to any of the physical development mechanisms described in section 1, the Th data for each TC are run through a low-pass digital filter with a cutoff period of 24 h.

The T_o − 36 h to T_o time window is chosen to represent the development period of the TC without extending the system back-trajectory beyond its range of applicability as noted in section 2b. Figure 4 shows the Q and Th time series plots for Hurricane Michael (2000) [Fig. 4 plots for Hurricane Claudette (2003) will be discussed later], representing a cyclogenesis event with strong baroclinic influence, using the terminology of Hess et al. (1995). The logarithmic normalization (n)

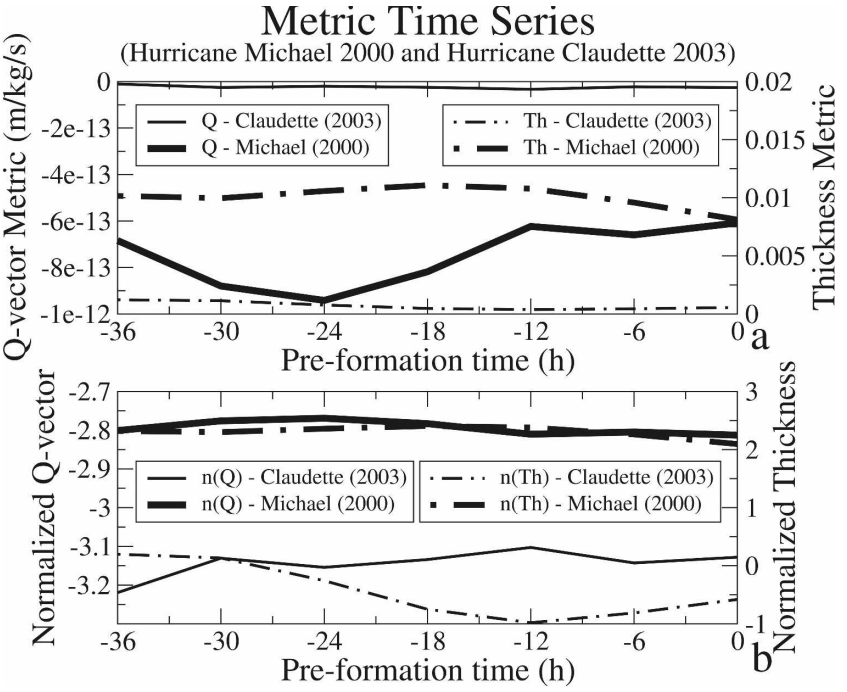

FIG. 4. Sample metric time series plots for Hurricanes Michael (2000) and Claudette (2003), as indicated in the legends on the graphs. (a) Raw metric values and (b) normalized metrics used for statistical processing for direct comparison with Figs. 7, 8. The notation $n(\,)$ is used in the legend of (b) to represent normalization as defined in (2) and (3). Note that the sign reversal for Q normalization in (2) means that stronger Q forcing results in mathematically larger $n(Q)$ values; however, $n(Q)$ remains below zero for all observed values of the metric.

undertaken in Fig. 4b accounts for the skewed nature of both the Q and the Th distributions (Figs. 5a,b), using

$$\tilde{Q} = n(Q) \equiv \frac{\ln(-Q)}{10} \quad \text{and} \tag{2}$$

$$\tilde{\text{Th}} = n(\text{Th}) \equiv \ln(\text{Th} \times 10^3), \tag{3}$$

respectively. These same transformations are made to the raw data prior to the application of the statistical model, making Fig. 4b useful for reference with the results of the classification scheme. The results of the normalization are shown in Figs. 5c,d. Note that the Q metric in Fig. 4 not only represents a strong forcing but also exhibits a large change in magnitude as the trough approaches and is weakened by the diabatic outflow from the developing TC. This serves as an example of why it is important to retain information about the evolution of the metrics during the classification process, rather than simply to study their maximum or mean values over the period. Similar sequences for Hurricane Claudette (2003), also shown in Fig. 4, document a development that follows a traditional tropical-only pathway (Hess et al. 1995) with low and nearly constant values for both metrics. Although unresolved structures fueling Claudette's cyclogenesis cannot be evaluated with the NCEP–NCAR reanalysis to allow for discrimination between the mesoscale flavors of the nonbaro-

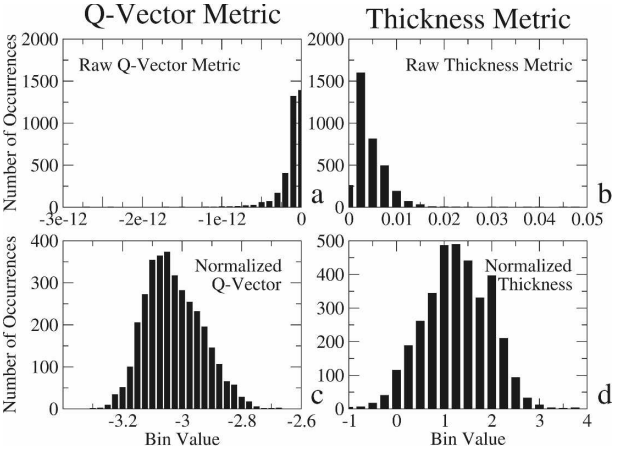

FIG. 5. Histograms of the computed (a) Q and (b) Th metrics for all events and all times from $T_o - 36$ h to T_o. The corresponding histograms of the metric values following the logarithmic normalizations defined in (2) and (3): (c) normalized Q vector and (d) normalized thickness.

clinic development pathways (section 1), these series highlight the dramatically different behaviors of the discriminants for these two fundamentally different development events.

If maximum or mean values of the metrics were sufficient to represent the physical processes important in distinguishing between the modes of tropical cyclogenesis, then a cluster analysis technique could be applied to identify favored regions on a two-dimensional (Q, Th) phase space that would represent the cyclogenesis categories. However, the handling of time-varying metrics complicates the problem by requiring a statistical method that groups similar trajectories through a set of phase spaces, one for each analysis time between T_o − 36 h and T_o.[7] For the time series plots (Fig. 4), this means that groups must be self-consistent in terms of not only the magnitude of the metrics but also the structure of their evolution over time (i.e., they have highly correlated time series).

The statistical technique employed to address this problem, and ultimately to generate the tropical cyclogenesis classification scheme, is called latent trajectory modeling (LTM; Lazarfeld and Henry 1968). This approach has received significant attention over the last decade as a model-based variant of nonhierarchical (single level) cluster-analysis methods. In this study, the trajectory (TRAJ) extension package for the statistical analysis system (SAS) is used for all LTM computations (Nagin 1999; Jones et al. 2001).

The key to any class-based analysis technique is the recognition that the observations (in this case, the time series of the metrics Q and Th) are drawn from an inhomogeneous population consisting of some finite number of latent classes. These classes are "latent" because they are not directly observed but are instead inferred from the set of chosen metrics (often called manifest variables in statistical studies). One of the attributes of LTM that makes it particularly applicable to this study is that the values of the metrics themselves are used to identify both the optimal number of individual groups (C_Q, C_{Th}, and $C = C_Q \times C_{\mathrm{Th}}$ for Q-based, Th-based, and total group numbers, respectively) and the characteristic trajectory (time series) for each of them. This allows us to remain consistent in our data-driven approach to the development of the classification scheme as displayed diagrammatically in Fig. 6. The diagnosed time series values of the metrics lead directly to an evaluation of the number and type of groups, along with an estimate of the proportion of cases that fall into the different categories. The derived parameters for each class are then used to compute the group membership of each storm. The relationships between each of the boxes in Fig. 6 will be described in the remainder of this section.

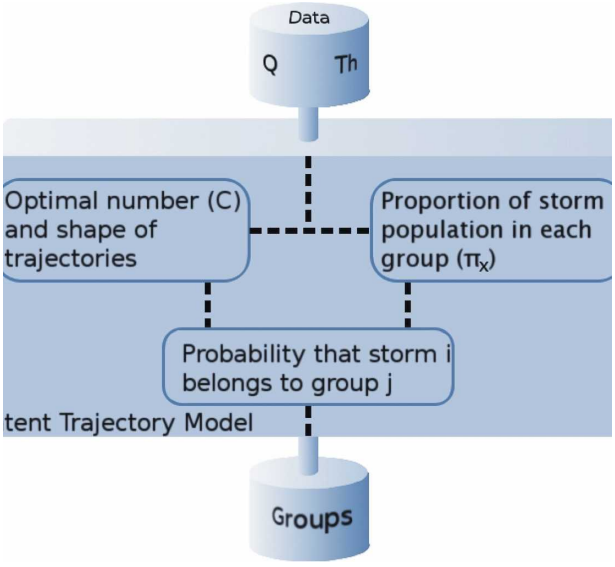

FIG. 6. Flow diagram for the LTM as applied in this study. The databases used for input and output are represented by cylinders, the LTM is shown with an encompassing cube, and data flow within the LTM is shown with dashed lines.

A normal distribution model is used to establish a connection between the predevelopment time $\alpha = \{T_o - 36\ \mathrm{h}, T_o - 30\ \mathrm{h}, \ldots, T_o\}$ (a series of length T) and the expected value of the metric. We will focus here on the Q metric for clarity; the application of the LTM approach for Th is similar. This model implies that each individual category (x) has an associated set of nth-order polynomial coefficients (β^x) that combine to yield q_{it}, the model estimate of the ith storm's value of Q at time t (where t is between T_o − 36 h and T_o),

$$q_{it}^x = \beta_0^x + \alpha_{it}\beta_1^x + \alpha_{it}^2\beta_2^x + \cdots + \alpha_{it}^n\beta_n, \qquad (4)$$

where α_{it} is the predevelopment time for TC i at time t. In this study, only first-order (linear) polynomial models are required to adequately fit the metric time series, so (4) reduces to

$$q_{it}^x = \beta_0^x + \alpha_{it}\beta_1^x. \qquad (5)$$

The fact that the model coefficients are allowed to vary with x (by group) is critical because this allows the model to detect heterogeneity (clustering) in the shapes of the metric time series.

[7] In statistical nomenclature, a "trajectory" corresponds to a meteorological time series. For example, the T_o − 36 h to T_o time series of Q is the trajectory for Q over the period.

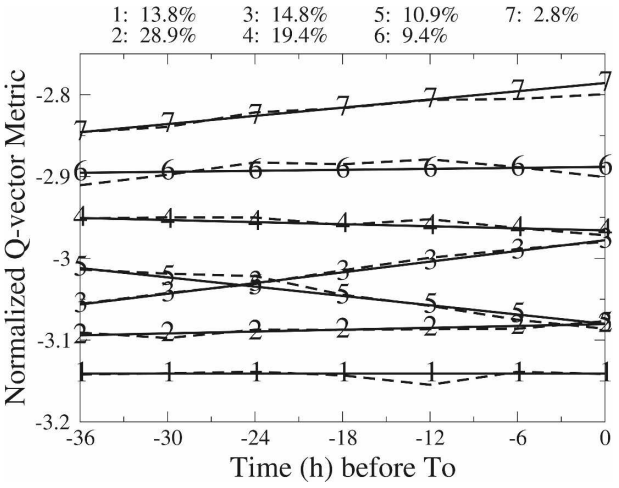

FIG. 7. Categories for the Q metric generated by the LTM. The mean trajectory for each group is plotted with a dashed line, and the model trajectory for the group is plotted with a corresponding labeled solid line. Membership percentages for each group are shown in the legend at the top of the plot, as in Table 2.

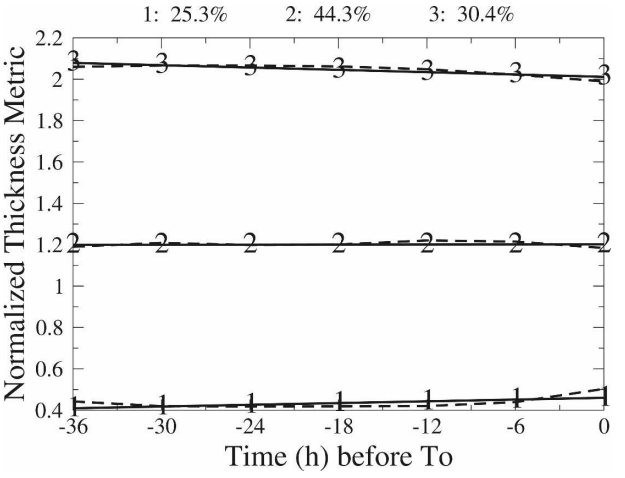

FIG. 8. Same as Fig. 7, but for the Th metric.

The time series of the diagnosed metric Q for storm i is denoted as

$$\mathbf{Q}_i = \{Q_{T_o - 36\,\mathrm{h}}, Q_{T_o - 30\,\mathrm{h}}, \ldots, Q_{T_o}\}. \tag{6}$$

The probability of computing the value of $\mathbf{Q}_i$ as described in section 2b, given storm i membership in group x, can be expressed as $\Pr^x(\mathbf{Q}_i)$. This probability is constructed for the normal distribution as

$$\Pr^x(\mathbf{Q}_i) = \prod_{t=1}^{T} \frac{1}{s}\,\phi\left(\frac{Q_{it} - q_{it}^x}{s}\right), \tag{7}$$

where Π is the product operator, ϕ is the probability density function of a normal random variable with a mean defined by (5) and a standard deviation of s, and T is the number of points in the trajectory (here, the number of 6-h time periods between $T_o - 36$ h and T_o). The overall probability of membership in group x (alternatively the fraction of TC genesis events that fall into that category) is given by π_x and will be one of the quantities computed by the LTM.

The likelihood (joint density) is the sum of the conditional likelihoods,

$$\Pr(\mathbf{Q}_i) = \sum_{x=1}^{C_Q} \pi_x \Pr^x(\mathbf{Q}_i), \tag{8}$$

and represents the unconditional probability of observing the ith TC's metric time series ($\mathbf{Q}_i$). The parameters of interest in the model (β_0^x, β_1^x, π_x and s) can be estimated by the maximization of the logarithm of $\Pr^x(\mathbf{Q}_i)$ (Nagin 1999; Jones et al. 2001). This maximization is performed using a general quasi-Newton procedure as described by Dennis et al. (1981). The optimal number of categories (C_Q) is determined using the Bayesian information criterion (D'Unger et al. 1998). Following the maximization of $\ln[\Pr^x(\mathbf{Q}_i)]$, each category defined by the Q metric has its own set of parameters. Using these groups to condition the TC events, a similar analysis is performed for the Th metric. The result of the LTM is a set of C groups, each possessing unique values of the shapes and magnitudes of their characteristic time series.

Figure 7 shows the mean trajectories of the seven independent groups defined by the LTM for the Q metric (dashed lines). Because of the (2) and (3) transformations, smaller values of the ordinate indicate weaker near-storm synoptic ascent forcing. Also shown in Fig. 7 are the models used to represent the characteristic trajectories of the categories, dependent on the β_0^x and β_1^x parameters in (5) (solid lines). The fraction of total tropical cyclogenesis events that falls into each group (π_x) is shown in Table 2. The three most weakly forced classes (groups 1, 2, and 5) describe over 53% of cases, while the three most strongly forced groups (4, 6, and 7) represent approximately 32% of storms. This indicates that while the majority of tropical cyclogenesis events evolve along a pathway with weak Q-vector forcing for ascent, a nonnegligible fraction—approximately one-third of all storms—develop in a near-storm environment that is influenced by sustained elevated values of the Q metric.

A similar set of trajectories for the Th metric is shown in Fig. 8. A pair of optimal classification schemes is found for the Th metric, one yielding three groups and the other producing seven. A manual inspection of the data cannot distinguish between the categories pro-

TABLE 2. Tropical cyclone membership percentage in each of the seven Q groups and the three Th groups, determined by the LTM analysis (Figs. 7, 8).

Metric	Group identifier	Membership percentage (π_x)	Summary description
Q	1	13.8	Constant low
	2	28.9	Constant low
	3	14.8	Medium, increasing toward T_o
	4	19.4	Constant medium
	5	10.9	Medium, decreasing toward T_o
	6	9.4	Constant high
	7	2.8	High, increasing toward T_o
Th	1	25.3	Constant low
	2	44.3	Constant medium
	3	30.4	Constant high

TABLE 3. Synthesis chart for recombination of LTM-derived categories to final tropical cyclogenesis categories.

Category	Membership percentage	Q group	Th group
Nonbaroclinic	40	1	1
		2	1
		5	1
		1	2
		2	2
		5	2
Low-level baroclinic	13	1	3
		2	3
		5	3
Transient–trough interaction	16	3	1
		3	2
		3	3
Trough induced	3	4	1
		6	1
		7	1
Weak TT	13	4	2
		6	2
		7	2
Strong TT	15	4	3
		6	3
		7	3

posed by the latter grouping strategy, so the optimal number of thickness asymmetry discriminated categories is taken to be three, representing low, moderate, and strong lower-level near-storm baroclinicity (a similar analysis using the full set of 591 Atlantic TCs from 1948 to 2005 also yielded a clear preference for three Th classes). Each of these groups shows very little change over the 36-h period leading up to T_o. The weak Th category represents 25.3% of tropical cyclogenesis events, while the moderate and strong Th classes comprose 44.3% and 30.4% of storms, respectively (Table 2).

4. Climatology results

The seven Q metric and three Th groups imply that each storm is a preferred member of 1 of 21 individual categories. A physically based synthesis of these groups is clearly necessary to reduce the number of classes to a reasonable value—one that allows for a manual discrimination of groups as described in section 1. The LTM framework allows for such a synthesis, provided that there is a clear physical basis for it. Table 3 documents the synthesis process used in this study, as the total number of TC genesis classes are reduced from 21 to 6. These six categories are nonbaroclinic, low-level baroclinic, transient–trough interaction, trough induced, weak TT, and strong TT. The fractional membership in each of these groups for the 496 storms in the study is shown in Table 3, and a categorized list of a sample of well-studied TCs is provided for reference in Table 4. A simplified schematic of the properties of the categories is shown in Fig. 9. This two-dimensional phase space—one dimension for each metric—is incapable of accurately depicting the evolutionary component of the analysis, but it is useful as a conceptual guide to the synthesized categories.

The largest proportion of events (40%) falls into the nonbaroclinic group (traditional "tropical developments" without the geographical constraints implied by the use of this term), indicating that nearly one-half of Atlantic TCs form in local environments with weak synoptic forcing and minimal lower-level baroclinicity. As shown in Figs. 10a, 11a, and Table 5, these systems tend to develop in the deep tropics west of 30°W during the peak of the Atlantic hurricane season. This region represents the central and western sections of the MDR, a region characterized by warm sea surface temperatures (SSTs) at the west end of the subtropical high. Storms in the nonbaroclinic group develop along one of the tropical pathways involving MCV development, hot tower spinup, vortex merger, stability profile modification, or surface flux enhancement, and likely a combination of several or all of these models (see section 1 for a review). As noted in section 2b, the resolution of the NCEP–NCAR reanalysis does not allow for discrimination between these mesoscale processes; however, the framework established here could readily be applied to further decompose the nonbaroclinic category in the future, given a reliable set of long-term mesoscale analyses and an appropriate additional metric.

The 13% of cases that are assigned to the low-level baroclinic category develop in areas with weak synoptic

TABLE 4. Categorized list of well-studied TCs, compared with subjective evaluations of cyclogenesis derived from the literature. Storms whose objective classification matches with the subjective grouping are highlighted in bold in the first column. For the purposes of this comparison, the transient–trough interaction and weak TT categories are considered subjectively equivalent since the distinction between them has not been previously recognized. Results of the objective classification for all storms in the 1948–2004 dataset can be found online (http://www.atmos.albany.edu/facstaff/rmctc/ttclim/indexd.php).

Storm name	Year	LTM classification	Subjective description (based on review of literature)	References
Hurricane Alberto	2000	Low-level baroclinic	Near-African wave development	Berry and Thorncroft (2005)
Tropical Storm Allison	2001	Weak TT*	Identified recent weak TT	Davis and Bosart (2004)
Hurricane Andrew	1992	Nonbaroclinic	Deep easterly wave development	Karyampudi and Pierce (2002)
Hurricane Arlene	1967	Nonbaroclinic	Long-lived easterly wave development	Carlson (1969)
Hurricane Beulah	1967	Nonbaroclinic	Long-lived easterly wave development	Carlson (1969)
Tropical Storm Chloe	1967	Low-level baroclinic	Near-African easterly wave development	Carlson (1969)
Hurricane Diana	1984	Strong TT*	The first well-documented strong TT	Davis and Bosart (2001, 2002)
Hurricane Dolly	1996	Nonbaroclinic	Multivortex tropical development	Reasor et al. (2005)
Hurricane Danny	1997	Nonbaroclinic	WISHE-based multivortex development	Molinari et al. (2004)
Tropical Storm Ernesto	1994	Nonbaroclinic	MLEJ-induced vortex superposition	Karyampudi and Pierce (2002)
Hurricane Florence	2000	Strong TT	Identified recent strong TT	Davis and Bosart (2004)
Hurricane Gabrielle	2001	Transient–trough interaction	Identified recent weak TT	Davis and Bosart (2004)
Hurricane Gustav	2002	Strong TT	Identified recent strong TT	Davis and Bosart (2004)
Hurricane Humberto	2001	Weak TT	Identified recent weak TT	Davis and Bosart (2004)
Hurricane Karen	2001	Strong TT	Identified recent strong TT	Davis and Bosart (2004)
Tropical Storm Leslie	2000	Strong TT	Identified recent weak TT	Davis and Bosart (2004)
Hurricane Luis	1995	Low-level baroclinic	MLEJ-induced vortex superposition	Karyampudi and Pierce (2002)
Hurricane Michael	2000	Strong TT	Identified recent strong TT	Davis and Bosart (2004)
Tropical Storm Nadine	2000	Transient–trough interaction	Identified recent weak TT	Davis and Bosart (2004)
Hurricane Olga	2001	Strong TT	Identified recent strong TT	Davis and Bosart (2004)

* Storm was excluded from the final dataset because of an initial strength above tropical storm (section 2), but it was classified based on an LTM analysis of the complete 591-storm 1948–2004 dataset.

forcing but strong lower-level baroclinicity. The bulk of events appear to follow the SAL/MLEJ pathway described in section 1. Figures 10b, 11b, and Table 5 demonstrate that these events cluster strongly in the Cape Verde region during August and September, with some additional developments occurring in the western Caribbean as a result of land–sea temperature differences in the area. The spatial locality suggests that the classification scheme is effective, since no geographical information was included in the development of the categories. It therefore appears that fundamentally different development mechanisms are at work in various parts of the basin (Gray 1968; Elsner et al. 1996) and that the proposed scheme is able to discriminate effectively between them.

The transient trough interaction category (16%) represents storms that undergo their early development from $T_o - 36$ h to about $T_o - 12$ h in a local environment devoid of strong synoptic forcing. Close to T_o, however, a strong Q-vector forcing pattern interacts with the incipient vortex. This may occur if a trough strikes the developing TC late in its development phase. These events tend to occur throughout the western MDR and in the Gulf of Mexico (Fig. 10c), particularly during the early portion of the season (Fig. 11c; Table 5) when troughs dip deeper into the tropics over relatively cool SSTs.

The trough-induced group, representing only 3% of all TC developments, is characterized by strong upper-

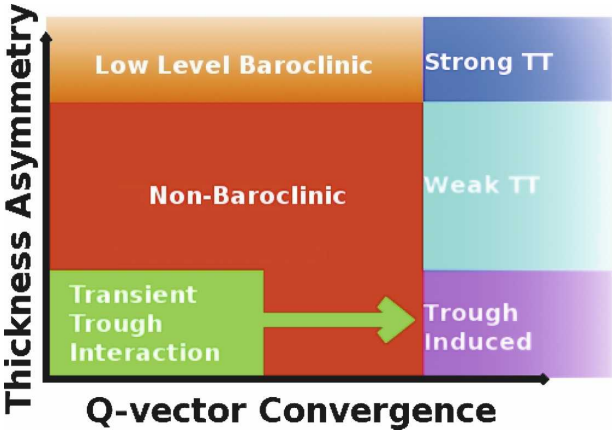

FIG. 9. Simplified description of LTM-derived tropical cyclogenesis categories in a two-dimensional phase space based on the Q and Th metrics. The significant temporal evolution of the Q metric over the $T_o - 36$ h to T_o period is depicted with a green arrow extending from the category base.

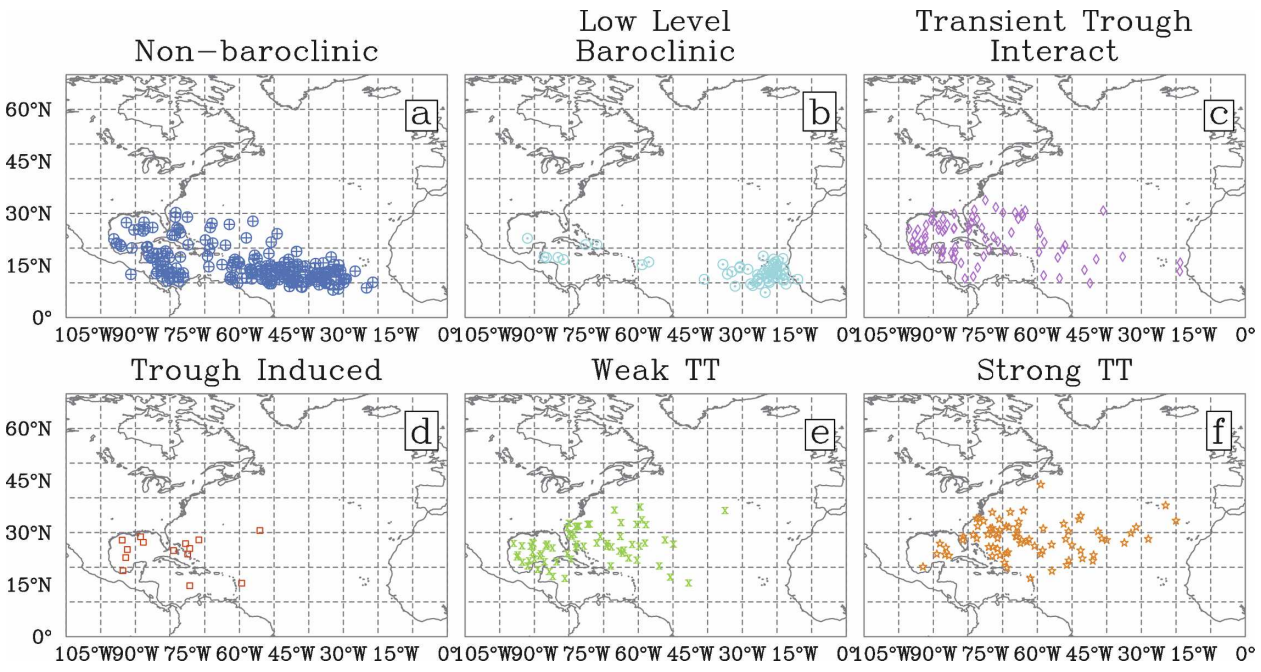

FIG. 10. Spatial distribution of tropical cyclogenesis (T_o) locations for all members of each category, as indicated by the title on the individual panels.

level forcing and very weak lower-level baroclinicity. These storms tend to occur in the Gulf of Mexico in August (Figs. 10d, 11d; Table 5), where the heat fluxes from uniformly warm SSTs modify the overlying lower atmosphere to eliminate baroclinicity, and strong trough penetrations from the North American continent are common late in the hurricane season. Sustained trough forcing acts through a deep layer in this destabilizing atmosphere, producing vertical motions that generate vorticity through lower-level conver-

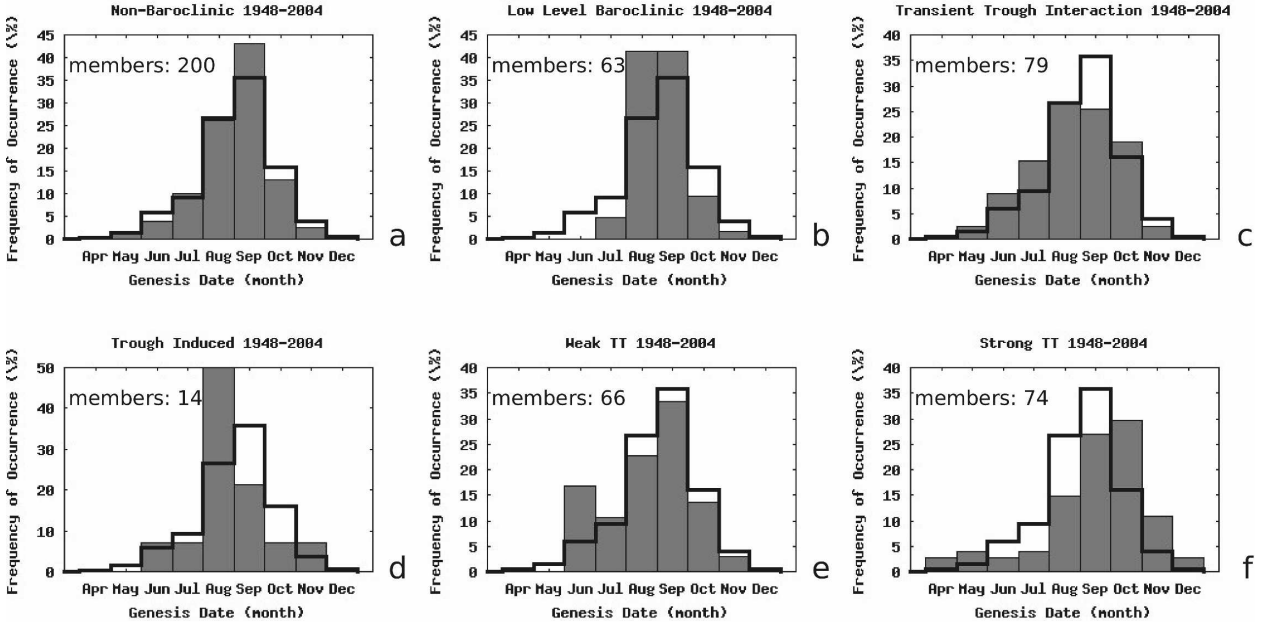

FIG. 11. Histograms of the relative monthly frequency of cyclogenesis events in each category (gray bars) as indicated by the title on the individual panels. The climatological cyclogenesis–frequency distribution for all 496 TCs is shown with a solid black line in each plot.

TABLE 5. Intraannual distribution of the number of tropical cyclogenesis events in each LTM-identified category.

Category	April	May	June	July	August	September	October	November	December
Nonbaroclinic	0	2	8	20	52	86	26	5	1
Low-level baroclinic*	0	0	0	3	26	26	6	1	0
Transient–trough interaction	0	2	7	12	21	20	15	2	0
Trough induced	0	0	1	1	7	3	1	1	0
Weak TT	0	0	11	7	15	22	9	2	0
Strong TT**	2	3	2	3	11	20	22	8	2
Total	2	7	29	46	132	177	79	19	3

* One low-level baroclinic event (unnamed storm) was recorded in February 1952.
** One strong TT event (Subtropical Storm 1) was recorded in January 1978.

gence. Mesoscale elements of the tropical development mechanisms described in section 1 are undoubtedly required to focus the broad ascent onto the vortex scale for development, but they are unresolved by the NCEP–NCAR reanalysis.

The weak TT (13%) and strong TT (15%) development categories represent TCs that are initiated under conditions of strong synoptic forcing (as for the trough-induced group) but with medium-to-high values of lower-level baroclinicity, respectively. These storms follow the TT development pathways described in section 1 and benefit from the presence of both upper- and lower-level cyclogenetic forcings. Weak TT events occur preferentially in the northern Gulf of Mexico and along the western subtropical Atlantic throughout the season (Figs. 10e, 11e; Table 5). Strong TTs form farther into the western and central Atlantic at higher latitudes (Fig. 10f), with above-climatological frequency in both the spring and the fall (Fig. 11e; Table 5). The timing and northerly position of these tropical cyclogenesis events suggest that they are less sensitive to suboptimal SST conditions because of the presence of the strong-trough anomaly aloft (Emanuel 2005) and ample opportunity for isentropic lift at lower and midlevels.

The track densities and individual tracks of the TCs in each category are shown in Figs. 12, 13. While storms in the nonbaroclinic group tend to have above-average

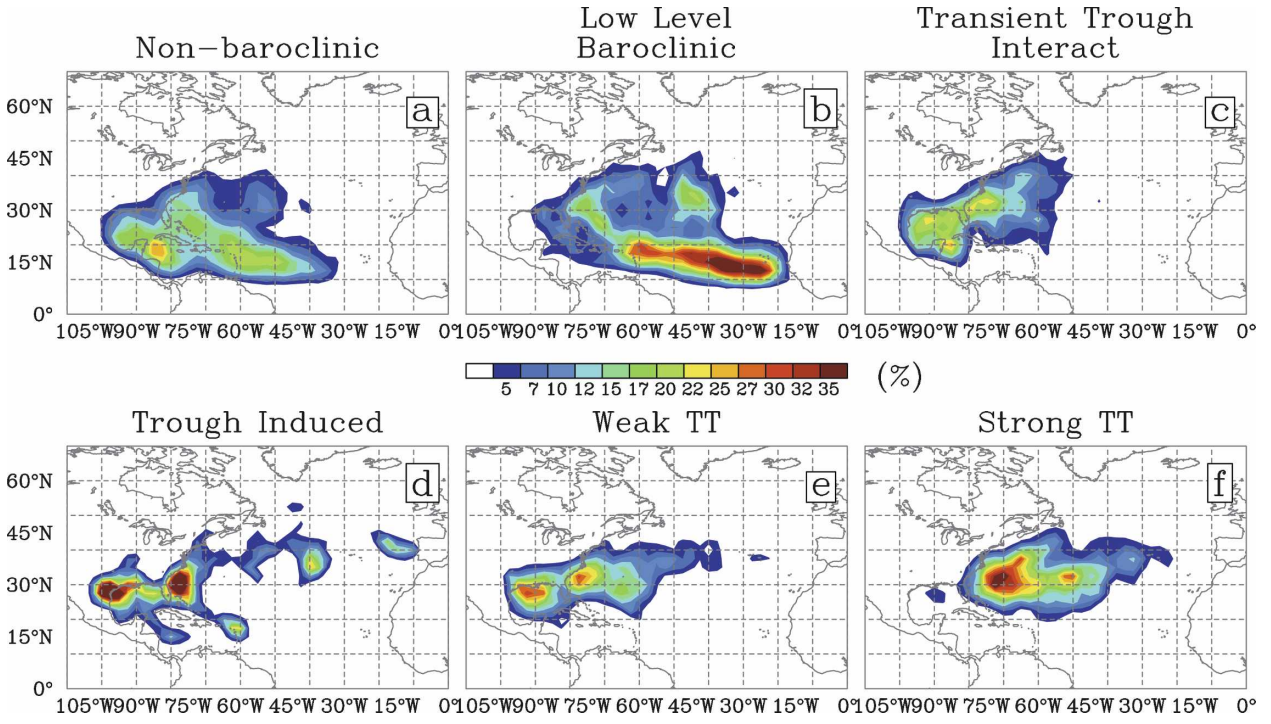

FIG. 12. As in Fig. 10, but for track densities computed on a 2.5° grid (same grid spacing as the original NCEP–NCAR reanalysis dataset).

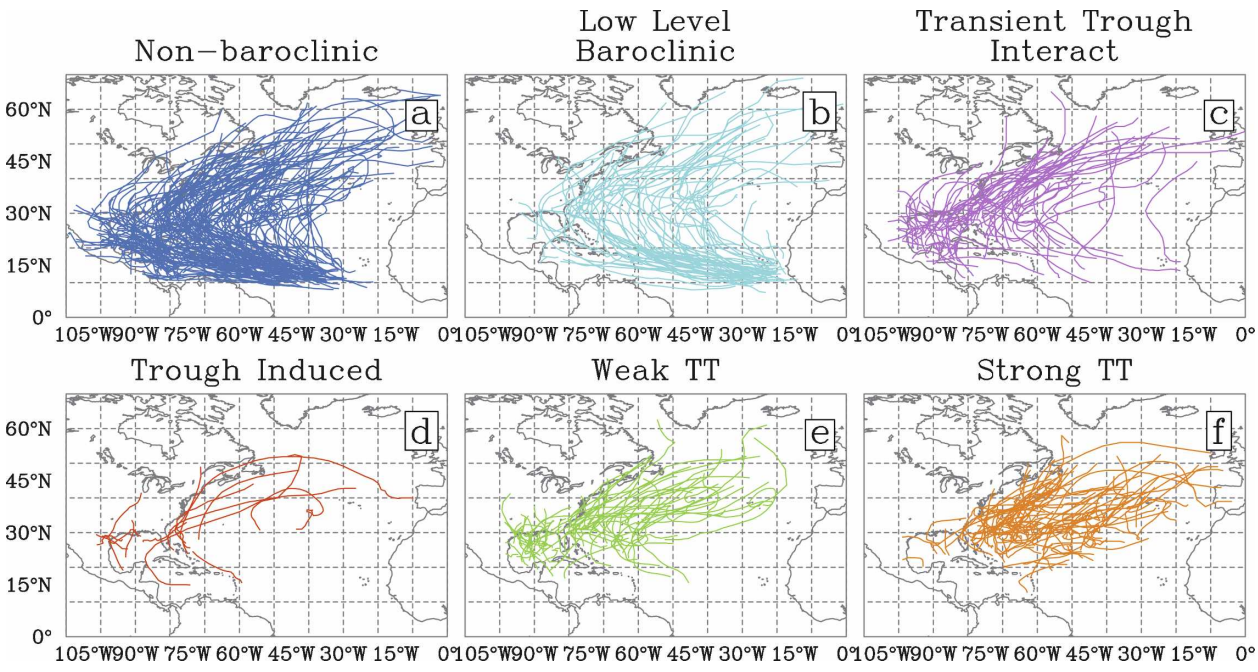

FIG. 13. As in Fig. 10, but for all TC tracks in each category.

length tracks (median track 4800 km), members of the low-level baroclinic class cover significantly longer distances (median track 6200 km). The other groups show consistently shorter track lengths (Table 6), and many of the storms in the TT categories begin near the point of recurvature (Figs. 13e,f). As noted with respect to geographical cyclogenesis clustering, the dramatic differences in the track density and TC path charts, combined with the statistical significance of the track length variations shown in Table 6, suggest that the proposed tropical cyclogenesis classification scheme is successfully identifying fundamentally different events.

Evidence of postgenesis life cycle differences between the categories is shown in Fig. 14 and Table 6 in the form of maximum TC intensity. The median peak intensity in the nonbaroclinic group is 39 m s^{-1}, significantly different from the climatological median of 36 m s^{-1} because of the large number of members in the group (Table 6). A bimodal behavior in the low-level baroclinic category (Fig. 14b) suggests that while some of this group's members fail to reach appreciable intensity, those that do are capable of generating very strong winds—the median peak intensity for this category is 46 m s^{-1}. This is consistent with the interpretation that the

TABLE 6. Tropical cyclone genesis month (Fig. 11), track length (Fig. 13), and peak wind speed (Fig. 14) summary statistics for the six tropical cyclogenesis categories and for the full 496-member set. The statistical significance of departures from the climatological distribution is computed using a Mann–Whitney (ranked sum) test and a 95% confidence threshold. The application of this nonparametric test is necessary because of the skewed nature of the compared distributions. The results shown in the genesis month columns are derived from a Mann–Whitney test performed on the genesis yeardate of each TC (with a base date of 1 January of the year in question) to avoid discrete monthly blocks that would result in an excessive number of ties during the ranking procedure.

		Genesis month		Track length		Peak wind speed	
Category	Members	Median	Significance	Median (km)	Significance	Median (m s^{-1})	Significance
All 496 tropical cyclones	496	September	—	3700	—	36	—
Nonbaroclinic	200	September	No	4800	Yes	39	Yes
Low-level baroclinic	63	September	No	6200	Yes	46	Yes
Transient–trough interaction	79	August	No	2900	Yes	34	No
Trough induced	14	August	No	3000	No	32	No
Weak TT	66	August/September	No	2100	Yes	30	Yes
Strong TT	74	September	Yes	3100	Yes	34	Yes

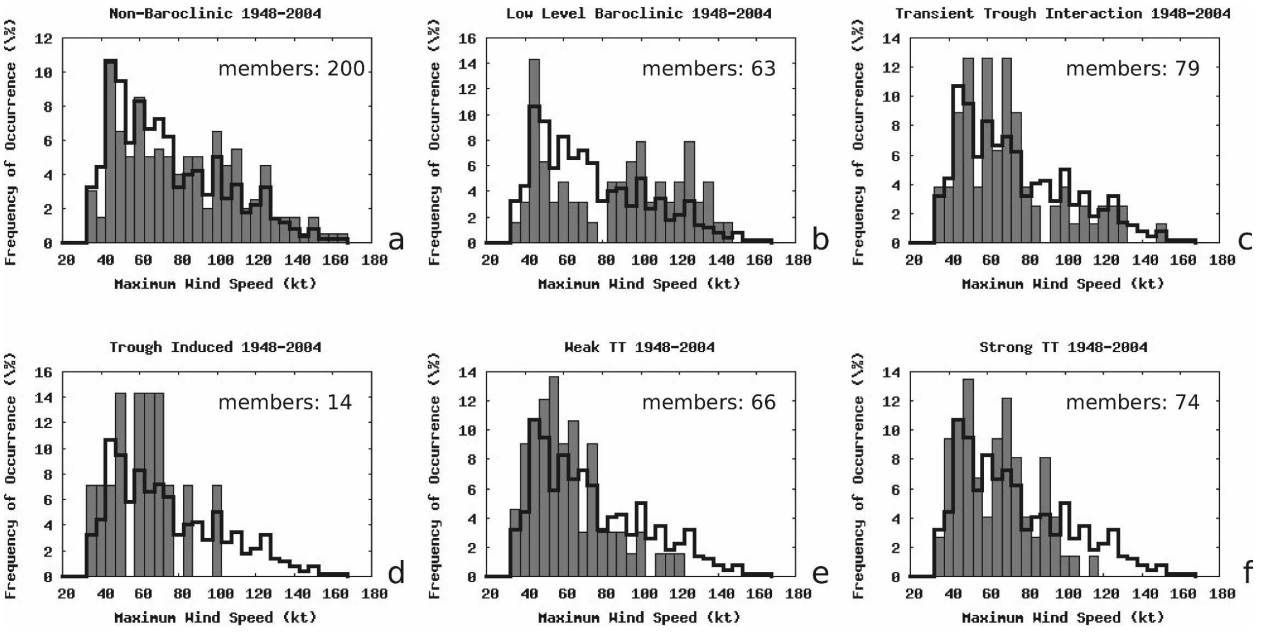

FIG. 14. As in Fig. 11, but for peak TC intensity.

low-level baroclinic group represents Cape Verde systems; however, the nonnormality of the distribution shown in Fig. 14b may be affected by the small 63-member sample size. The remaining classes show weaker peak intensities relative to the climatology, with the most notable examples of this behavior evident in the TT categories (Figs. 14e,f). The differences in the evolutions of the TCs in the individual groups suggest that storms that form following different pathways exhibit different behaviors throughout their life cycles. The extent to which this is a function of the TC formation location as opposed to structure will be investigated in a subsequent compositing study based on the categorized dataset.

Further indications of the success of the objective classification scheme include the evaluation presented in Table 4, in which 18 of the 20 selected storms match the subjective development pathways described in the literature, and a direct comparison with the results of Hess et al. (1995). In that study, the authors find that 49% of North Atlantic TCs form as tropical-only storms while 51% undergo baroclinically influenced developments over the 1950–93 period. Combining the nonbaroclinic and low-level baroclinic groups into a tropical-only proxy and assigning the remaining LTM-identified classes to the Hess et al. (1995) category, a 1950–93 subset of this study identifies 52% tropical-only and 48% baroclinically influenced development events. The close agreement between the two studies, whose methodologies differ dramatically, lends additional credibility to the objective scheme described here, inasmuch as it appears, on average, to be capable of reproducing independent subjective analyses of the TC-development mode.

5. Summary and discussion

Landfalling hurricanes are among the deadliest and costliest frequently occurring natural disasters in the world. Although significant advances have been made recently in the forecasting of TC tracks, both academic and operational groups continue to address the challenges of tropical development and intensity prediction. The former issue is addressed here through the establishment of an objective tropical cyclogenesis classification scheme.

Field campaigns and high-resolution modeling investigations have led to the development of many theories concerning the nature of tropical cyclogenesis over the last decade. This study uses the NCEP–NCAR reanalysis to develop a dynamically based climatology of tropical cyclogenesis in the North Atlantic. The coarse resolution of the gridded dataset—combined with its questionable reliability in tropical oceanic regions during periods of rapid evolution associated with the initiation phase of a poorly sampled tropical vortex—does not permit distinction between the purely tropical modes of cyclogenesis, most of which differ from each other in mesoscale structure and through processes that occur on the scale of the incipient MCV itself. However, an

appropriate choice of discriminant variables allows the NCEP–NCAR reanalysis to distinguish between identifiable pathways of TC genesis when forcings from the near-storm environment exert a notable influence on the nature of the development.

Measures of the local quasi-nondivergent Q-vector forcing for ascent (Q) and the lower-level baroclinicity (Th) are found to be optimal choices for metrics based on an extensive analysis of cases from the 1948–2004 period of the climatology. The Q metric increases in value with additional ascent forcing, generally driven by the presence of an upper-level trough of midlatitude origin. This discriminant also doubles as a proxy for the poorly represented midlevel moisture field, since regions of sustained synoptic-scale ascent exhibit increased values of relative humidity compared to their local environments because of the adjustment of the thermal profile. The Th metric increases in value with increased near-storm baroclinicity, thereby permitting the identification of tropical cyclogenesis events where lower-level isentropic ascent plays a role in enhancing development. This discriminant is maximized in cases involving remnant midlatitude circulations and the MLEJ west of Africa.

Time series for each storm-centered metric for all 496 storms from the NHC best- track archive are generated for the period from $T_o - 36$ h to T_o. This allows for the retention of information not only about the magnitude of the metrics for each TC but also about their evolution over the period of tropical development. The LTM statistical technique is used to analyze these time series results by grouping them into a number of categories determined by the data themselves. Each resulting class of storms contains events with similar values and structures of the metric time series and therefore is dynamically self-consistent with respect to the chosen discriminants.

A physically based synthesis of the 21 categories found by the LTM allows the groups to be combined into six readily identifiable classes of tropical cyclogenesis: nonbaroclinic, low-level baroclinic, transient–trough interaction, trough induced, weak TT, and strong TT. Although the largest proportion of events falls into the nonbaroclinic category, a nonnegligible number of events is also identified for each of the other classes of development. Analysis of the formation locations of the six groups shows that there is a remarkable degree of geographic separation, given that no positional data are available to the LTM during its development of the classification scheme. The track behaviors of the grouped TCs also appear to be significantly different from each other in some cases. These preliminary results suggest that this scheme succeeds in grouping TC developments in a dynamically consistent manner and that the flavor of tropical cyclogenesis can have a significant impact on the subsequent evolution of the system.

This climatology extends the study of Elsner et al. (1996) by utilizing the dynamic and thermodynamic information contained in the NCEP–NCAR reanalysis. There are many potential applications for the classification scheme described here. An investigation of the life cycles of systems in the individual TC categories will be the focus of a future study and may yield useful diagnostic and predictive results. The transformation of this scheme into a real-time product may provide forecasters with additional stratified climatology information of potential use for evaluating model performance based on historical experience. The ability of global and regional climate models to simulate realistic hurricanes could be evaluated by classifying storms using this scheme, for comparison with the climatology results. As higher-resolution analysis and reanalysis datasets become available, this flexible methodology can be extended to identify mesoscale features and forcings that distinguish between events in the tropical development class consistent with the conceptual models reviewed in section 1, thereby allowing for the continued study of tropical cyclogenesis from an increasingly detailed climatological perspective.

Acknowledgments. The authors thank John Gyakum and Eyad Atallah for useful discussions during the course of this study. This work was supported by NSF Grant ATM-0304254.

REFERENCES

Adams, J. C., and P. N. Swarztrauber, 1997: SPHEREPACK 2.0: A model development facility. NCAR Tech. Note NCAR/TN-436-STR, 58 pp.

Berry, G. J., and C. Thorncroft, 2005: Case study of an intense African easterly wave. *Mon. Wea. Rev.,* **133,** 752–766.

Bister, M., and K. A. Emanuel, 2002: Low frequency variability of tropical cyclone potential intensity 1. Interannual to interdecadal variability. *J. Geophys. Res.,* **107,** 4801, doi:10.1029/2001JD000776.

Bosart, L. F., and J. A. Bartlo, 1991: Tropical storm formation in a baroclinic environment. *Mon. Wea. Rev.,* **119,** 1979–2013.

Bracken, W. E., and L. F. Bosart, 2000: The role of synoptic-scale flow during tropical cyclogenesis over the North Atlantic Ocean. *Mon. Wea. Rev.,* **128,** 353–376.

Burpee, R. W., J. L. Franklin, S. J. Lord, R. E. Tuleya, and S. D. Aberson, 1996: The impact of Omega dropwindsondes on operational hurricane track forecast models. *Bull. Amer. Meteor. Soc.,* **77,** 925–933.

Carlson, T. N., 1969: Synoptic histories of three African disturbances that developed into Atlantic hurricanes. *Mon. Wea. Rev.,* **97,** 256–276.

——, and J. M. Prospero, 1972: The large-scale movement of Sa-

haran air outbreaks over the northern equatorial Atlantic. *J. Appl. Meteor.,* **11,** 283–297.

Chapman, S., and R. S. Lindzen, 1970: *Atmospheric Tides: Thermal and Gravitational.* D. Reidel, 201 pp.

Charney, J. G., and M. E. Stern, 1962: On the stability of internal baroclinic jets in a rotating atmosphere. *J. Atmos. Sci.,* **19,** 159–172.

Chen, S. S., and W. M. Frank, 1993: A numerical study of the genesis of extratropical convective mesovortices. Part I: Evolution and dynamics. *J. Atmos. Sci.,* **50,** 2401–2426.

Dai, A., and J. Wang, 1999: Diurnal and semidiurnal tides in the global surface pressure fields. *J. Atmos. Sci.,* **56,** 3874–3891.

Davis, C., and L. F. Bosart, 2001: Numerical simulations of the genesis of Hurricane Diana (1984). Part I: Control simulation. *Mon. Wea. Rev.,* **129,** 1859–1881.

——, and ——, 2002: Numerical simulations of the genesis of Hurricane Diana (1984). Part II: Sensitivity of track and intensity prediction. *Mon. Wea. Rev.,* **130,** 1100–1124.

——, and ——, 2004: The TT problem. *Bull. Amer. Meteor. Soc.,* **85,** 1657–1662.

——, and ——, 2006: The formation of Hurricane Humberto (2001): The importance of extra-tropical precursors. *Quart. J. Roy. Meteor. Soc.,* **132,** 2055–2086.

DeMaria, M., M. Mainelli, L. K. Shay, J. A. Knaff, and J. Kaplan, 2005: Further improvement to the Statistical Hurricane Intensity Prediction System (SHIPS). *Wea. Forecasting,* **20,** 531–543.

——, J. A. Knaff, and C. Sampson, 2007: Evaluation of long-term trends in tropical cyclone intensity forecasts. *Meteor. Atmos. Phys.,* **97,** 19–28.

Dennis, J. E., Jr., D. M. Gay, and R. E. Welsch, 1981: An adaptive nonlinear least-squares algorithm. *Proc. Annu. Conf. Assoc. Cumput. Mach. Trans. Math. Software,* **7,** 348–383.

Dong, K., and C. J. Neumann, 1986: The relationship between tropical cyclone motion and environmental geostrophic flows. *Mon. Wea. Rev.,* **114,** 115–122.

D'Unger, A., K. Land, P. McCall, and D. Nagin, 1998: How many latent classes of delinquent/criminal careers? Results from mixed Poisson regression analyses of the London, Philadelphia, and Racine cohorts studies. *Amer. J. Socio.,* **103,** 1593–1630.

Dvorak, V. F., 1975: Tropical cyclone intensity analysis and forecasting from satellite imagery. *Mon. Wea. Rev.,* **103,** 420–430.

Eady, E., 1949: Long waves and cyclone waves. *Tellus,* **1,** 33–52.

Elsberry, R. L., G. J. Holland, H. Gerrish, M. DeMaria, and C. P. Guard, 1992: Is there any hope for tropical cyclone intensity prediction? *Bull. Amer. Meteor. Soc.,* **73,** 264–275.

Elsner, J. B., G. S. Lehmiller, and T. B. Kimberlain, 1996: Objective classification of Atlantic hurricanes. *J. Climate,* **9,** 2880–2889.

Emanuel, K. A., 2005: Genesis and maintenance of "Mediterranean hurricanes." *Adv. Geosci.,* **2,** 1–4.

——, and R. Rotunno, 1989: Polar lows as arctic hurricanes. *Tellus,* **41,** 1–17.

Goerss, J. S., 2007: Prediction of consensus tropical cyclone track forecast error. *Mon. Wea. Rev.,* **135,** 1985–1993.

Goldenberg, S. B., and L. J. Shapiro, 1996: Physical mechanisms for the association of El Niño and West African rainfall with Atlantic major hurricane activity. *J. Climate,* **9,** 1169–1187.

Gray, W., 1968: Global view of the origin of tropical disturbances and storms. *Mon. Wea. Rev.,* **96,** 669–700.

Hart, R. E., 2003: A cyclone phase space derived from thermal wind and thermal asymmetry. *Mon. Wea. Rev.,* **131,** 585–616.

Hendricks, E. A., M. T. Montgomery, and C. A. Davis, 2004: The role of "vortical" hot towers in the formation of Tropical Cyclone Diana (1984). *J. Atmos. Sci.,* **61,** 1209–1232.

Hess, J. C., J. B. Elsner, and N. E. LaSeur, 1995: Improving seasonal hurricane predictions for the Atlantic basin. *Wea. Forecasting,* **10,** 425–432.

IWTC-VI, 2006: Summary of major recommendations from IWTC-VI. Sixth World Meteorological Organization Int. Workshop on Tropical Cyclones Tech. Rep., 14 pp. [Available online at http://severe.worldweather.org/iwtc.]

Jones, B. L., D. S. Nagin, and K. Roeder, 2001: A SAS procedure based on mixture models for estimating developmental trajectories. *Socio. Methods Res.,* **29,** 374–393.

Kalnay, E., and Coauthors, 1996: The NCEP/NCAR 40-Year Reanalysis Project. *Bull. Amer. Meteor. Soc.,* **77,** 437–471.

Karyampudi, V. M., and H. F. Pierce, 2002: Synoptic-scale influence of the Saharan air layer on tropical cyclogenesis over the eastern Atlantic. *Mon. Wea. Rev.,* **130,** 3100–3128.

Kistler, R., and Coauthors, 2001: The NCEP–NCAR 50-Year Reanalysis: Monthly means CD-ROM and documentation. *Bull. Amer. Meteor. Soc.,* **82,** 247–267.

Knabb, R. D., J. R. Rhome, and D. P. Brown, 2005: Tropical cyclone report: Hurricane Katrina. National Hurricane Center, National Oceanographic and Atmospheric Administration Tech. Rep., 43 pp. [Available online at http://www.nhc.noaa.gov/2005atlan.shtml.]

Landsea, C. W., 2007: Counting Atlantic tropical cyclones back to 1900. *Eos, Trans. Amer. Geophys. Union,* **88,** 197–208.

Lazarsfeld, P. F., and N. W. Henry, 1968: *Latent Structure Analysis.* Houghton Mifflin, 294 pp.

Lindzen, R. S., and S.-S. Hong, 1974: Effects of mean winds and horizontal temperature gradients on solar and lunar semidiurnal tides in the atmosphere. *J. Atmos. Sci.,* **31,** 1421–1446.

Maddox, R. A., 1983: Large-scale meteorological conditions associated with midlatitude, mesoscale convective complexes. *Mon. Wea. Rev.,* **111,** 1475–1493.

Marks, F. D., L. K. Shay, and PDT-5, 1998: Landfalling tropical cyclones: Forecast problems and associated research opportunities. *Bull. Amer. Meteor. Soc.,* **79,** 305–323.

McTaggart-Cowan, R., E. H. Atallah, J. R. Gyakum, and L. H. Bosart, 2006: Hurricane Juan (2003). Part I: A diagnostic and compositing life cycle study. *Mon. Wea. Rev.,* **134,** 1725–1747.

Miller, B. I., 1958: The use of mean layer winds as a hurricane steering mechanism. U.S. National Hurricane Research Project Tech. Rep. 18, 24 pp.

Molinari, J., D. Vollaro, and K. L. Corbosiero, 2004: Tropical cyclone formation in a sheared environment: A case study. *J. Atmos. Sci.,* **61,** 2493–2509.

Montgomery, M. T., M. E. Nicholls, T. A. Cram, and A. B. Saunders, 2006: A vortical hot tower route to tropical cyclogenesis. *J. Atmos. Sci.,* **63,** 355–386.

Nagin, D. S., 1999: Analyzing developmental trajectories: A semiparametric, group-based approach. *Psychol. Methods,* **4,** 139–157.

Newton, C. W., 1966: Circulations in large sheared cumulonimbus. *Tellus,* **18,** 699–712.

Nielsen-Gammon, J. W., and D. A. Gold, 2008: Dynamical diagnosis: A comparison of quasigeostrophy and Ertel potential vorticity. *Fred Sanders: A Tribute to His Influence on Weather Analysis and Forecasting, and His Legacy of Teaching, Meteor. Monogr.,* No. 55, Amer. Meteor. Soc., in press.

NOAA, 2006: NOAA predicts very active 2006 North Atlantic hurricane season. National Oceanographic and Atmospheric

Administration. [Available online at http://www.noaanews.noaa.gov/stories2006/s2634.htm.]

Pasch, R. J., E. S. Blake, H. D. Cobb III, and D. P. Roberts, 2005: Tropical cyclone report: Hurricane Wilma. National Hurricane Center, National Oceanographic and Atmospheric Administration Tech. Rep., 27 pp. [Available online at http://www.nhc.noaa.gov/2005atlan.shtml.]

Phillips, N. A., 1958: Geostrophic errors in predicting the Appalachian storm of November 1950. *Geophysica,* **6,** 389–405.

Raymond, D. J., and H. Jiang, 1990: A theory for long-lived mesoscale convective systems. *J. Atmos. Sci.,* **47,** 3067–3077.

Reasor, P. D., M. T. Montgomery, and L. F. Bosart, 2005: Mesoscale observations of the genesis of Hurricane Dolly (1996). *J. Atmos. Sci.,* **62,** 3151–3171.

Ritchie, E. A., and G. J. Holland, 1993: On the interaction of two tropical cyclone scale vortices. II: Discrete vortex patches. *Quart. J. Roy. Meteor. Soc.,* **119,** 1363–1379.

——, and ——, 1997: Scale interactions during the formation of Typhoon Irving. *Mon. Wea. Rev.,* **125,** 1377–1396.

Rotunno, R., and K. A. Emanuel, 1987: An air–sea interaction theory for tropical cyclones. Part II: Evolutionary study using a nonhydrostatic axisymmetric numerical model. *J. Atmos. Sci.,* **44,** 542–561.

Sadler, J. C., 1976: A role of the tropical upper tropospheric trough in early season typhoon development. *Mon. Wea. Rev.,* **104,** 1266–1278.

——, 1978: Mid-season typhoon development and intensity change and the tropical upper tropospheric trough. *Mon. Wea. Rev.,* **106,** 1137–1152.

Shih, Y.-S., 1993: Tree-structured classification. Ph.D. thesis, University of Wisconsin—Madison, 161 pp.

Simpson, J., E. Ritchie, J. Holland, J. Halverson, and S. Stewart, 1997: Mesoscale interactions in tropical cyclone genesis. *Mon. Wea. Rev.,* **125,** 2643–2661.

——, J. B. Halverson, B. S. Ferrier, W. A. Petersen, R. H. Simspon, R. Blakeslee, and S. L. Durden, 1998: On the role of "hot towers" in tropical cyclone formation. *Meteor. Atmos. Phys.,* **67,** 15–35.

Simpson, R. H., and H. Riehl, 1981: *The Hurricane and Its Impact.* Louisiana State University Press, 398 pp.

Sippel, J. A., J. W. Nielsen-Gammon, and S. E. Allen, 2006: The multiple-vortex nature of tropical cyclogenesis. *Mon. Wea. Rev.,* **134,** 1796–1814.

Smith, C. D., 1950: The destructive storm of November 25–27, 1950. *Mon. Wea. Rev.,* **78,** 204–209.

Wallace, J. M., and R. F. Tadd, 1974: Some further results concerning the vertical structure of atmospheric tidal motions within the lowest 30 kilometers. *Mon. Wea. Rev.,* **102,** 795–803.

Warn, T., O. Bokhove, T. G. Shepherd, and G. K. Vallis, 1995: Rossby number expansions, slaving principles, and balance dynamics. *Quart. J. Roy. Meteor. Soc.,* **121,** 723–739.

Weisman, M. L., and J. B. Klemp, 1982: The dependence of numerically simulated convective storms on vertical wind shear and buoyancy. *Mon. Wea. Rev.,* **110,** 504–520.